3. STRUCTURAL ANALYSIS

3.1 USE OF COMPUTER SOFTWARE

The finite-element analysis (FEA) computer code used to analyze the 5-HLW/DOE SNF Long waste package with the FFTF DOE SNF canister in the center is ANSYS version V5.4. ANSYS V5.4 is identified with the CSCI 30040 V5.4 and is obtained from SCM in accordance with appropriate procedures. ANSYS V5.4 is a commercially available FEA code. ANSYS V5.4 software is qualified as documented in the Software Qualification Report (SQR) for ANSYS V5.4 (CRWMS M&O 1998j). ANSYS V5.4 is also referred to as ANSYS.

3.2 STRUCTURAL DESIGN ANALYSIS

Finite-element solutions resulted from structural analyses for the components of the 5-HLW/DOE SNF Long waste package. A detailed description of the finite-element representations, the method of solution, and the results are provided in CRWMS M&O (1998b). The results of these analyses are compared to the design criteria obtained from the 1995 American Society of Mechanical Engineers (ASME) Boiler and Pressure Vessel Code (BPVC), Section III, Subsection NB (ASME 1995), so that conclusions can be drawn regarding the structural performance of the 5-HLW/DOE SNF Long waste package design.

The design approach for determining the adequacy of a structural component is based on the stress limits given in the 1995 ASME BPVC. S_u is defined as the ultimate tensile strength of the materials, and S_m is defined as the design stress intensity of the materials. Table 3-1 summarizes design criteria as obtained from appropriate sections of the 1995 ASME BPVC.

Table 3-1. Containment Structure Allowable Stress-Limit Criteria

Category	Containment Structure Allowable Stresses	
	Normal Conditions (ASME 1995, Division 1, Subsection NB, Articles NB-3221.1 and NB-3221.3)	**Accident Conditions** (Plastic Analysis, ASME 1995, Division 1, Appendix F, Article F-1341.2)
Primary Membrane Stress Intensity	S_m	$0.7S_u$
Primary Membrane and Bending Stress Intensity	$1.5S_m$	$0.9S_u$

This analysis is within the bounds of the structural criteria from the SDD (CRWMS M&O 1998h) and does not consider other DBEs (e.g., crane two-block events), which are considered non-credible.

3.3 CALCULATIONS AND RESULTS

3.3.1 Description of the Finite-Element Representation

A two-dimensional (2-D) finite-element representation of the 5-HLW/DOE SNF Long waste package is developed to determine the effects of loads from the tipover DBE on the structural

components. The representation of the waste package includes the outer and inner barriers, the basket, the support tube, the DOE SNF canister and its basket and support tube, and the HLW pour canisters. This representation corresponds to a 2-D (x-y) slice from the middle of the waste package. After a tipover DBE onto an unyielding surface, the waste package lies horizontally as shown in Figure 3-1. A half-symmetry finite-element representation of the waste package was used. The barriers are assumed to have solid connections at the adjacent surfaces (Assumption 2.3.1.1) and are constrained in a direction perpendicular to the symmetry plane. For the first of the finite-element representations, the DOE SNF canister is included as a point mass at the bottom of the waste package support tube (the waste package lies horizontally), and no credit is taken for its structure. Therefore, the resulting closure of gap between the support tube and the DOE SNF canister is realistically calculated. If it is determined that the gap is not closed, there will be no structural load transferred from the support tube to the DOE SNF canister. Since all calculations are 2-D, masses per unit length are calculated based on the maximum allowable weight limits. Although the weight limit for the DOE SNF canister is 2,721 kg (DOE 1998b), the maximum weight limit from the SDD (CRWMS M&O 1998h), which is 3,400 kg, is used to calculate the stresses. Therefore, actual deformations will be smaller than the ones reported in this technical report.

For the second part of the calculations, the finite-element representation is modified to take structural credit for the DOE SNF canister and basket components. This representation is used to determine the maximum closure of the clearance gaps inside the FFTF DFA and the Ident-69 fuel pin container. The deformation values can then be compared to the fuel-assembly and the Ident-69 pin container dimensions to determine if there is contact between these components and the basket-structure.

First, the impact velocity of the inner lid's outer surface is calculated for a waste package tipover DBE. Then, this velocity is conservatively used in the 2-D finite-element analysis. Since the 2-D representation does not model a lid, the calculations will indicate that the waste package components undergo more deflection and stress than would actually occur. The target surface is conservatively assumed to be essentially unyielding by using a large elastic modulus for the target surface compared to the waste package (Assumption 2.3.1.2). The target surface is constrained at the bottom to prevent horizontal and vertical motion. Contact elements are defined between the top HLW pour canister and the inner brackets, and between the outer barrier and the target surface. Initial configuration of the finite-element representation includes a negligibly small gap for each contact element defined in the representation. This configuration allows enough time and displacement for the waste package and its internals to ramp up to the specified initial velocity before the impact. With this initial velocity, the simulation is then continued through the impact until the waste package begins to rebound. At that time, the stress peaks and the maximum displacements have been obtained.

The vitrified HLW glass material properties are represented by ambient material properties of general borosilicate glass. This document does not specifically report any results for the HLW glass canisters.

3.3.2 Results with No Credit for the Structural Components of the DOE SNF Canister

The first finite-element representation does not take structural credit for the DOE SNF canister; the mass is included by using a point mass element at the lowest point inside the support tube. The structural response of the waste package to tipover accident loads is reported using maximum stress values and displacements obtained from the finite-element solution to the problem. The results indicate that the maximum deformation inside the waste package support tube is 32.3 mm (CRWMS M&O 1998b, p. 13). Available space between the support tube and the DOE SNF canister is 44.3 mm (CRWMS M&O 1998b, p. 13). Hence, there will be no interference between the two components because of tipover DBE. The stresses on the waste package components and the DOE SNF canister are shown in Figure 3-1. Table 3-2 presents the stresses in each component of the waste package, and shows that the inner barrier of the waste package will not breach since the peak stresses are below the $0.9S_u$ which is the ASME code allowance stress limit shown in Table 3-1.

Table 3-2. 5-HLW/DOE SNF Long Waste Package FEA Stress Results

Component	Ultimate Tensile Strength (MPa)	$0.7S_u$, (MPa)	$0.9S_u$, (MPa)	Maximum Stress Intensity (MPa)	Maximum Membrane Stress (MPa)	Maximum Membrane Plus Bending Stress (MPa)
Outer barrier	483	338	435	372	25	486
Inner barrier	690	483	621	418	412	418
Basket plates and support tube	483	338	435	474	27	555

3.3.3 Results with Structural Credit for the DOE SNF Canister Components

The maximum deformation causing cavity closure around the fuel assembly is determined for the case of 5-HLW waste package representation that includes the structural components of the DOE SNF canister. The displacement results of the waste package tipover structural analysis showed that the maximum FFTF DFA cavity closure is 7.3 mm due to the deformation of the DOE SNF canister basket (CRWMS M&O 1998b, p. 13). The available gap between the FFTF DFA and the basket is 11.6 mm (CRWMS M&O 1998b, p. 13). Therefore, the DFA will not be crushed by the basket structure.

Similarly, the maximum deformation inside the Ident-69 container shell is determined to be 12.8 mm (CRWMS M&O 1998b, p. 13). On the other hand, available space between the FFTF DOE SNF canister center tube and the Ident-69 pin container is 11.7 mm (see CRWMS M&O 1998b, p. 13). This seems to result in an interference (1.1 mm) between these two parts due to impact. This is an artifact of the computational representation. The case was setup with the DOE SNF canister in contact with the waste package basket (support tube), which simplifies the calculations and reduces computing time. Since the 44.3 mm gap between the DOE SNF canister and the waste package support tube was not utilized, a significant part of the load that deformed the support tube in the waste package basket was transmitted directly to the DOE SNF canister and its basket structure in this representation. This causes excessive deformation of the DOE SNF canister basket and appears to trap the Ident-69 pin container in the center tube. As shown in Section 3.3.2, since the gap between the DOE SNF canister and the waste package

support tube does not fully close, there is no load transferred to the DOE SNF canister and its basket. Thus the deformation will be much less and there will be no interference between any of the fuel-assemblies or the Ident-69 container and the basket structure.

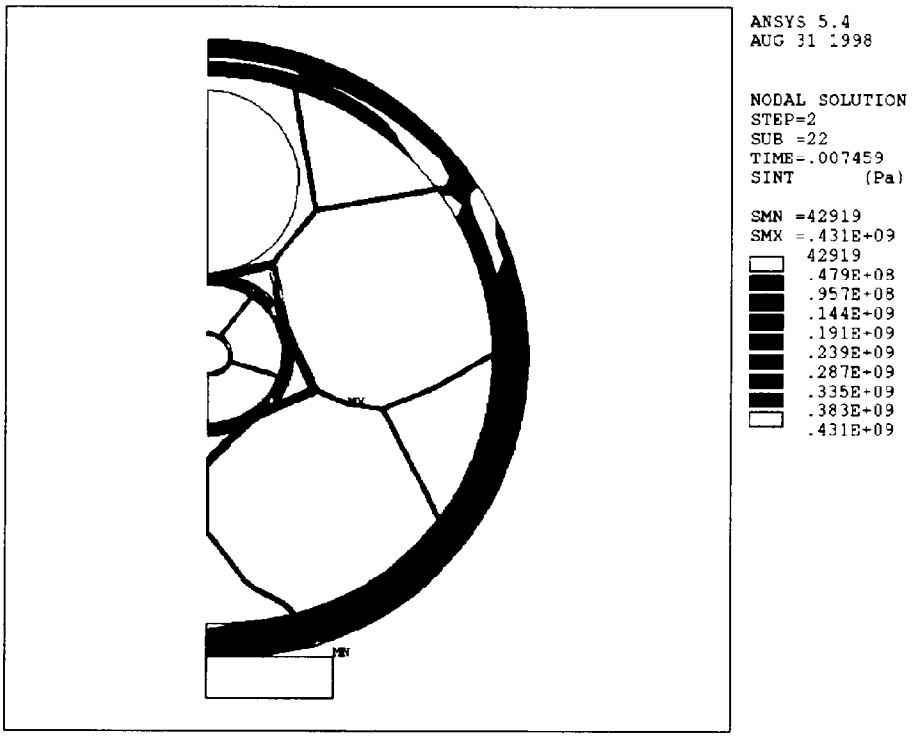

Figure 3-1. Stresses in 5-HLW/DOE SNF Long Waste Package

3.4 SUMMARY

The results given in Section 3.3 show that there is sufficient clearance between the inner diameter of the support tube and the outer diameter of the DOE SNF canister in the case of a tipover DBE. Hence, there will be no interference between the two components, and the DOE SNF canister can be removed from the support tube if needed to be set inside another waste package.

4. THERMAL ANALYSIS

4.1 USE OF COMPUTER SOFTWARE

The FEA computer code used to analyze the 5-HLW/DOE SNF Long waste package containing an FFTF DOE SNF canister is ANSYS Version V5.4. ANSYS V5.4 is identified as CSCI 30040 V5.4 and is obtained from SCM in accordance with appropriate procedures. ANSYS is a commercially available finite-element thermal- and mechanical-analysis code. ANSYS V5.4 software is qualified as documented in the SQR for ANSYS V5.4 (CRWMS M&O 1998j). ANSYS V5.4 is also referred to as ANSYS.

4.2 THERMAL DESIGN ANALYSIS

A detailed description of the finite-element representations, the method of solution, and the results are provided in CRWMS M&O (1999b). Each DFA and the Ident-69 fuel pin container holds 217 fuel pins in this representation. The FFTF standard DFA representation in this calculation is a 2-D section of the hexagonal duct containing 217 pins, as shown in Figures 2-6 and 2-7. The wire spacers around each fuel pin are conservatively neglected in this calculation (wire spacers provide contact and thus increase the transfer of thermal energy by conduction to the outside), so that the pins are represented as floating within the driver duct. In this analysis, the axial cross section at the center of the fuel pin is represented.

The cross section of the Ident-69 fuel pin container is shown in Figure 2-9. For this calculation, which represents a loading of 217 pins, the pins are consolidated loosely into the container, and therefore, are allowed to settle. The pins are considered packed together near the center of the container. In reality, the settled configuration of the pins would vary a great deal between each of the six partitioned sections. However, in this analysis, the settled configuration of fuel pins is represented as a constant since this approach simplifies the calculation and is considered conservative.

As shown in Figure 2-1, the waste package outside of the support tube for the DOE SNF canister is divided into five sections by the plates of the waste package basket. The plates of the FFTF DOE SNF canister also divide the space around the central support tube for the Ident-69 container into five sections. Due to this symmetry, thermal conditions within each of the five sections (representing 72° of the entire 360° of the waste package) will be approximately the same. In addition, within each of the 72° sections, the waste package components possess a further radial line of symmetry. Therefore, transient conditions in the waste package can be represented by one-tenth of the total radial geometry (a 36° slice of the full 360°) as shown in Figure 4-1.

The waste package outside of the Ident-69 fuel pin container is divided evenly into 72° slices, but the interior of the Ident-69 container is symmetrically divided by 60° slices. For this reason, the interior of the Ident-69 fuel pin container cannot be accurately included in the same 36°-slice finite-element representation as the waste package outside of the Ident-69. The calculation is therefore divided into two parts, corresponding to the two parts of the finite-element representation.

Figures 4-1 and 4-2 give the designated node locations and numbers on each component of the finite-element representations. Note that the outer shell of the Ident-69 fuel pin container is included, in Part 1 of the finite-element representation.

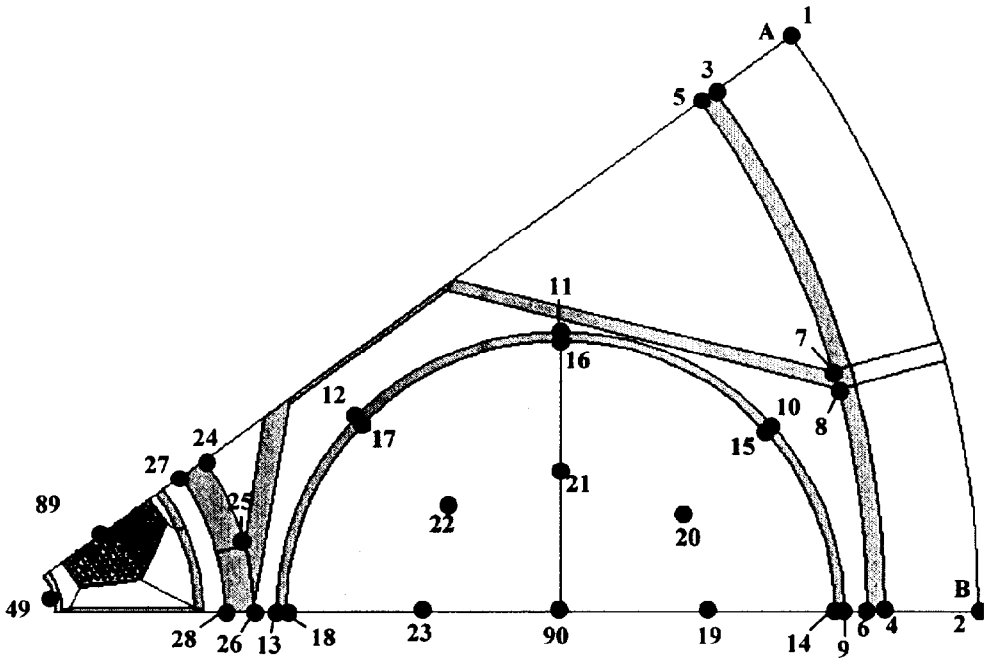

Figure 4-1. Node Locations and Numbers on Part 1 of the Finite-element Representation (WP Basket and Hanford 15 ft HLW Canister)

Two cases are considered, one with helium as the fill gas for the FFTF DOE SNF canister and the other with argon as the fill gas. The final fuel irradiations in FFTF were completed in March 1992 (INEEL 1998). Therefore, in all cases, the FFTF fuel is represented after ten years from discharge. The waste package total heat output is 13,533 W, and is based on five HLW glass canisters, five DFAs, and one Ident-69 pin container (Ident-69 pin container heat output is the same as one DFA).

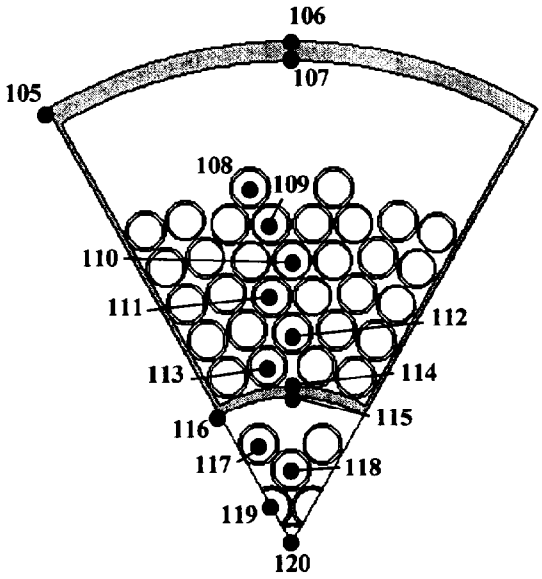

Figure 4-2. Node Locations and Numbers on Part 2 of the Finite-element Representation (Ident-69 Fuel Pin Container)

4.3 CALCULATIONS AND RESULTS

Table 4-1 lists the physical location of the most important nodes shown in Figures 4-1 and 4-2. Figure 4-3 shows the surface and peak fuel temperatures calculated in each case. The temperature distribution in the waste package at the time of peak fuel temperature can be found in CRWMS M&O (1999b), Attachments XIV through XVII. Table 4-2 summarizes the peak temperatures and time of occurrence for each case. The results indicate that argon fill gas in the FFTF DOE SNF canister causes the peak fuel temperature, which occurs after nine years, to be approximately 1.5% higher than helium fill gas. The peak HLW glass and waste package surface temperatures are not affected by the choice of the fill gas in the FFTF DOE SNF canister.

Table 4-1. Physical Locations of Nodes of Interest

Node Number	Physical Location
2	WP outer surface
90	HLW center
89	Standard DFA center fuel pin
49	Ident-69 outer surface, given as output of FEA, Part 1
106	Ident-69 outer surface, given as input to FEA, Part 2
120	Ident-69 center fuel pin

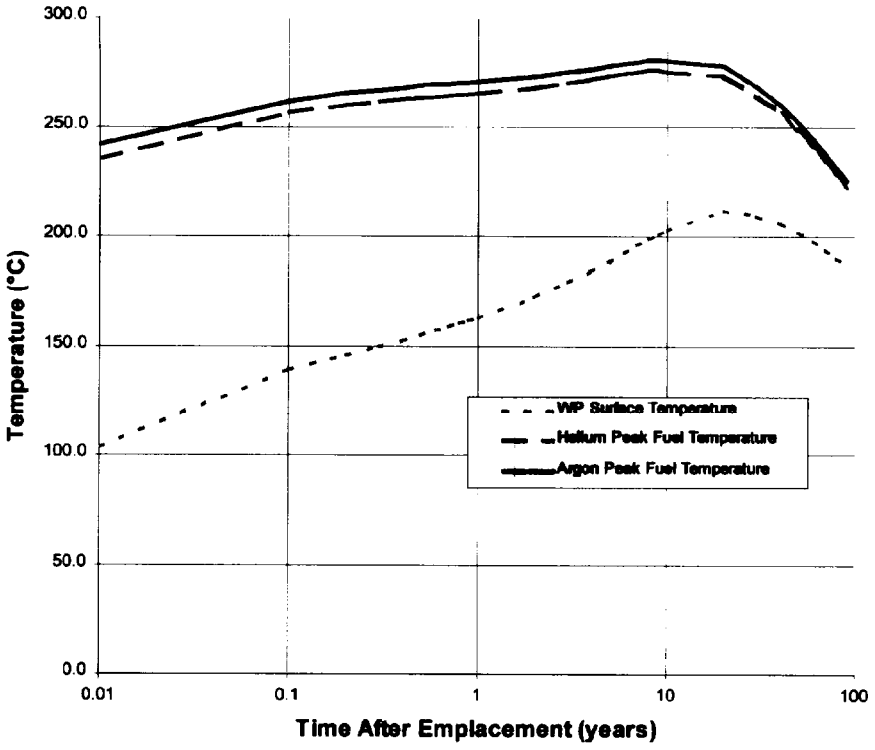

Figure 4-3. Temperature History for FFTF Codisposal WP

Table 4-2. Peak Temperatures and Time of Occurrence for Each Case

Case; FFTF DOE SNF Canister Fill Gas	Peak Fuel Temperature (°C)	Time of Peak Fuel Temperature (yr)	Peak Surface Temperature (°C)	Time of Peak Surface Temperature (yr)	Peak HLW Glass Temperature (°C)	Time of Peak HLW Glass Temperature (yr)
1; Helium	276.0	9	211.7	20	247.6	20
2; Argon	280.3	9	211.7	20	247.6	20

4.4 SUMMARY

The results indicate that the maximum fuel and HLW glass temperatures occur with argon fill gas in the DOE SNF canister and are 280.3 °C and 247.6 °C, respectively.

5. SHIELDING ANALYSIS

5.1 USE OF COMPUTER SOFTWARE

The Monte Carlo radiation transport code, MCNP, Version 4B2, is used to calculate average dose rates on the surfaces of waste package. This code identified as CSCI 30033 V4B2LV was previously obtained from the SCM in accordance with appropriate procedures. MCNP software is qualified as documented in the SQR for the MCNP, Version 4B2 (CRWMS M&O 1998i).

5.2 DESIGN ANALYSIS

The Monte Carlo method for solving the integral transport equation, which is implemented in the MCNP computer program, is used to calculate radiation dose rates for the waste packages. MCNP is set to use continuous-energy cross sections processed from the evaluated nuclear data files ENDF/B-V (LANL 1997, App. G). These cross section libraries are part of the qualified MCNP code system (CSCI 30033 V4B2LV). The flux averaged over a surface is tallied and the neutron and gamma flux to dose rate conversion factors (LANL 1997, App. H) are applied to obtain surface dose rates.

5.3 CALCULATIONS AND RESULTS

Dose rate calculations are performed for four cases: a waste package containing SRS HLW glass and FFTF fuel, a waste package containing only SRS HLW glass, a waste package containing Hanford HLW glass and FFTF fuel, and a waste package containing only Hanford HLW glass. All calculations use the glass composition given in Section 2.1.7. These calculations evaluated dose rates on all barrier boundaries of the waste package. Details of the calculations and the results for all cases considered are given in CRWMS M&O (1998c). The geometric representation, which ignores the waste package basket, for the MCNP calculations is shown in Figure 5-1. The surface-dose rates of the waste package containing Hanford HLW glass are approximately 20% higher than those of the waste package containing SRS glass. In addition, only the dose rates on the outer surfaces of the waste package are of most interest. Therefore, only the results from Hanford cases on these surfaces of interest are summarized and analyzed in detail.

Figure 5-2 shows the segments and surfaces of interest. Segment c is a 600 mm long radial surface segment axially centered at the middle of glass canisters. Segment a_1 is a 30-degree wide angular segment of the 600 mm long radial surface (segment c) near glass canisters. Segment b_1 is a 30-degree wide angular segment of the 600 mm long radial surface (segment c) near the gap between glass canisters. Segment d is an axial surface segment centered at the center of the waste package (Figure 5-3).

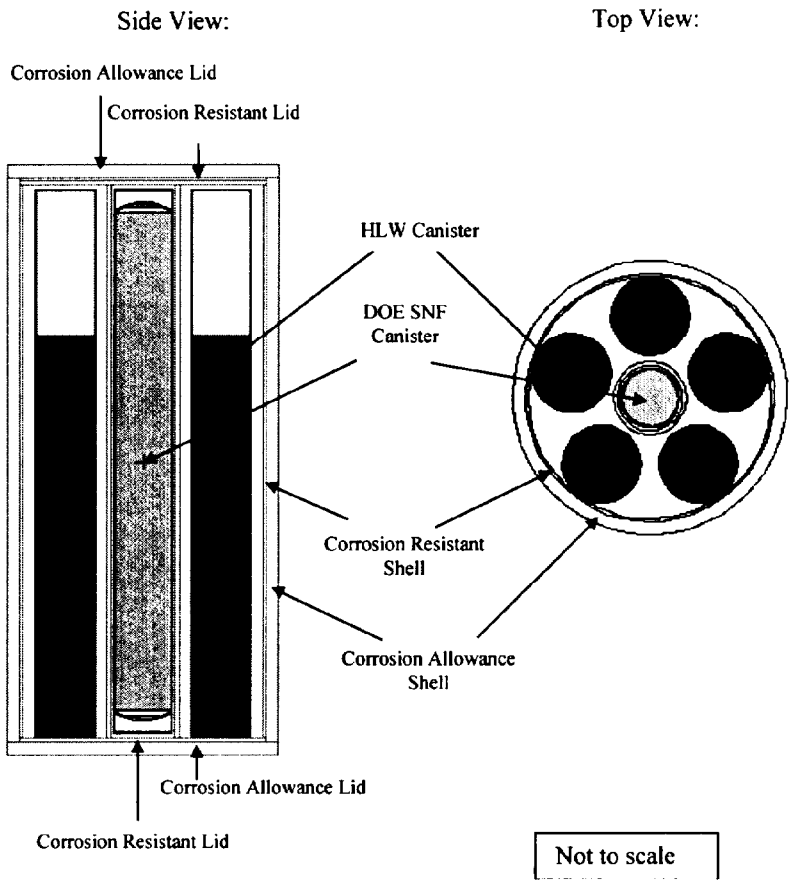

Figure 5-1. Vertical and Horizontal Cross Sections of MCNP Geometry Representation

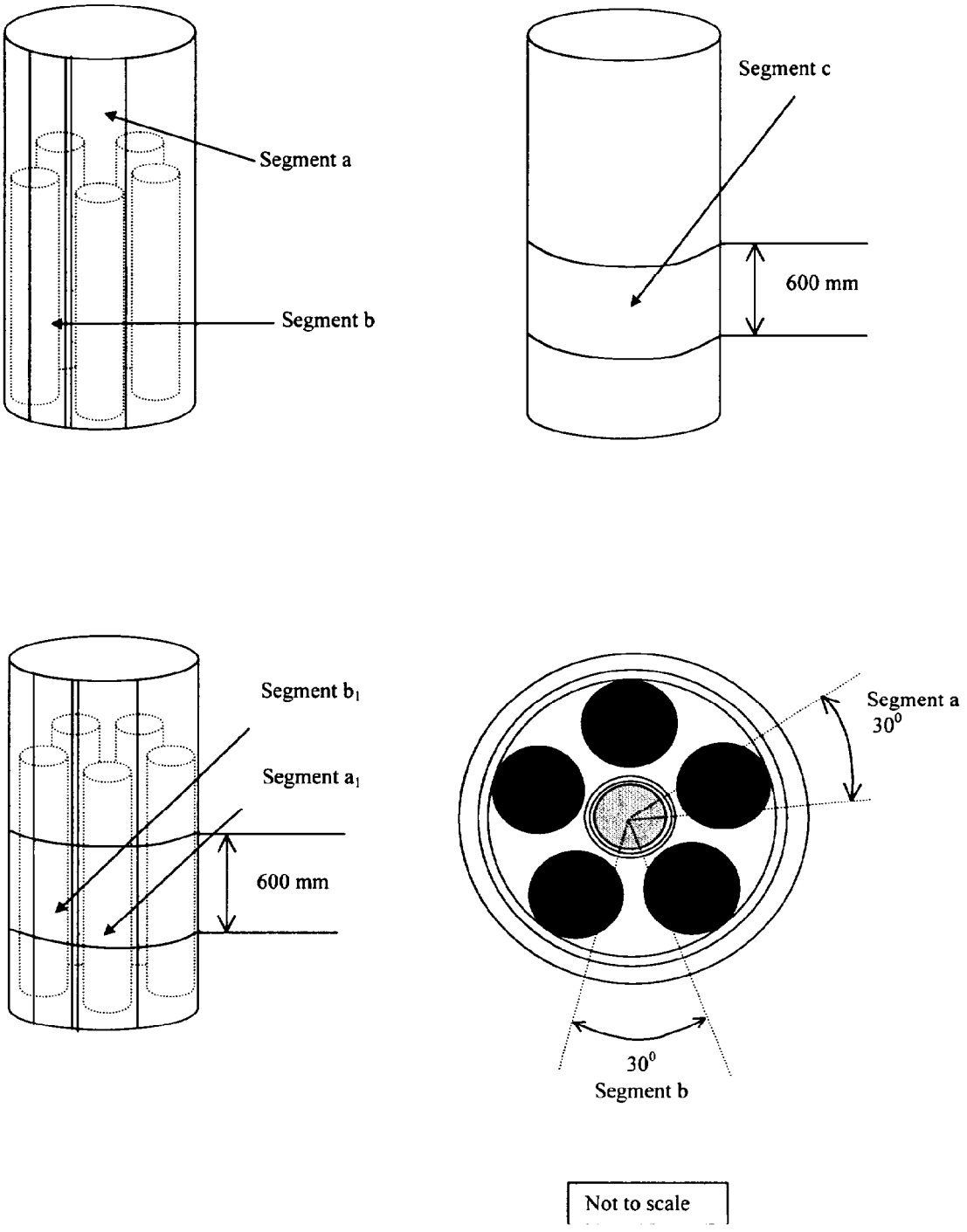

Figure 5-2. Radial Segments Used for Dose-Rate Calculations

5.3.1 Waste Package Containing Hanford HLW and FFTF Fuel

Tables 5-1 and 5-2 show the dose rates in rem/h on the surfaces of interest of the waste package containing the Hanford HLW glass and FFTF DOE SNF canister.

Table 5-1. Total Radial Dose Rates Averaged over a Height of 60 cm

Radial Position	Angular Position					
	Segment a_1		Segment b_1		Segment c	
	Dose Rate (rem/h)	Relative Error	Dose Rate (rem/h)	Relative Error	Dose Rate (rem/h)	Relative Error
Inner surface of inner barrier	9328.1	0.0246	9869.5	0.0238	9967.3	0.0086
Outer surface of outer barrier	15.9	0.0603	15.0	0.0716	15.0	0.0184

Table 5-2. Dose Rates in rem/h Averaged over Segment d

Axial Surface	Gamma Dose Rate (rem/h)	Relative Error	Neutron Dose Rate (rem/h)	Relative Error	Total Dose Rate (rem/h)	Relative Error
Outer surface of outer barrier bottom lid	1.52	0.1514	2.84E-02	0.0089	1.55	0.1486
Outer surface of outer barrier top lid	1.47	0.1317	1.28E-02	0.0131	1.48	0.1306

5.3.2 Waste Package Containing Only Hanford HLW

Tables 5-3 and 5-4 show dose rates on the surfaces of interest of the waste package containing the Hanford HLW glass only.

Table 5-3. Radial Gamma Dose Rates in rem/hr Averaged over a Height of 60 cm

Radial position	Angular Position					
	Segment a_1		Segment b_1		Segment c	
	Dose Rate (rem/h)	Relative Error	Dose Rate (rem/h)	Relative Error	Dose Rate (rem/h)	Relative Error
Inner surface of inner barrier	9.3928E+03	0.0219	1.0099E+04	0.0237	9.9595E+03	0.0070
Outer surface of outer barrier	15.83	0.0507	13.73	0.0679	14.45	0.0159

Table 5-4. Dose Rates in rem/h Averaged over Segment d

Axial Surface	Gamma Dose Rate (rem/h)	Relative Error
Outer surface of outer barrier bottom lid	3.11	0.1462
Outer surface of outer barrier top lid	1.57	0.2212

5.4 SUMMARY

The results of dose rate calculations are analyzed for the cases containing Hanford HLW and FFTF fuel, since that case has the highest dose rate among all cases investigated. Maximum dose rate on the outer surfaces of waste package is below 355 rem/h for all cases investigated. The highest dose rate of 15.9 ± 1.9 rem/h (uncertainties reported correspond to two standard deviations) is calculated on the 600 mm long, 30-degree wide angular segment of radial outer surface of the waste package (Segment a_1, see Figure 5-2). The primary gamma dose rate dominates the neutron dose rate by approximately three orders of magnitude.

The axial dose rates are higher on the bottom surfaces of waste packages because the HLW canisters rest on the bottom lids. The average dose rates on the outside of outer barrier of the bottom lid and the outside of the outer barrier of the top lid are 1.52 ± 0.46 rem/h and 1.47 ± 0.39 rem/h, respectively.

The dose on Segment a_1 is primarily due to the gamma rays of the adjacent HLW glass canister, while the dose on Segment b_1 is a contribution of gamma rays emitted from nearby HLW glass canisters. Source strength, geometry, and spectrum lead to a uniform angular dose over the radial surfaces of the waste packages for all analyzed cases.

The contribution to the total dose rate by the FFTF DOE SNF canister is approximately 10% for the waste package containing SRS HLW glass and approximately 5% for the waste package containing Hanford HLW glass. Figure 5-3 shows the MCNP estimates for dose rates over axial surfaces and segments in rem/h. The first value of each set is the surface dose rate for the waste package containing Hanford HLW glass and FFTF DOE SNF canister, while the second value is the surface dose rate for the waste package containing only Hanford HLW glass. The axial dose rate on Surface 10 (the inner surface of the inner barrier of the top lid) is about one order of magnitude lower than the axial dose rate on Surface 6 (inner surface of inner barrier bottom lid). The difference indicates that the doses on the axial surfaces are mainly due to HLW glass canisters. The upper surface of HLW glass canisters is about 1 m below the inner top lid and their bottom surfaces lay on the inner bottom lid, while the FFTF DOE SNF canister is symmetrically positioned at the center of the waste package.

The peak dose on the outside of top and bottom waste package outer lids (Figure 5-3, Segment d) is mainly produced by the gamma rays emitted in the HLW glass. The gamma rays from the HLW glass undergo multiple collisions and lose energy in the FFTF fuel and in the walls of the DOE SNF canister. The spectrum of gamma rays that enter the FFTF DOE SNF canister and then reach the Segment d of Surface 6 (see figure 5-3) is much softer than that of the gamma rays that travel through the less dense material of the HLW glass and reach the surrounding axial surface. The dose rate on Segment d is doubled when the FFTF DOE SNF canister is removed, indicating that its presence in the center of the waste package actually reduces the axial dose rates. This is mainly due to the fact that placing the FFTF DOE SNF canister in the center of the waste package provides shielding for the gamma rays from the HLW glass, which otherwise would only attenuate through air (or a fill gas) with a much smaller attenuation coefficient. The combined dose rate due to the gamma rays from the HLW glass that are shielded by the FFTF DOE SNF canister, and the gamma rays from the FFTF DOE SNF canister itself is, therefore,

less than the dose rate due to the gamma rays from the HLW glass in the absence of the FFTF DOE SNF canister.

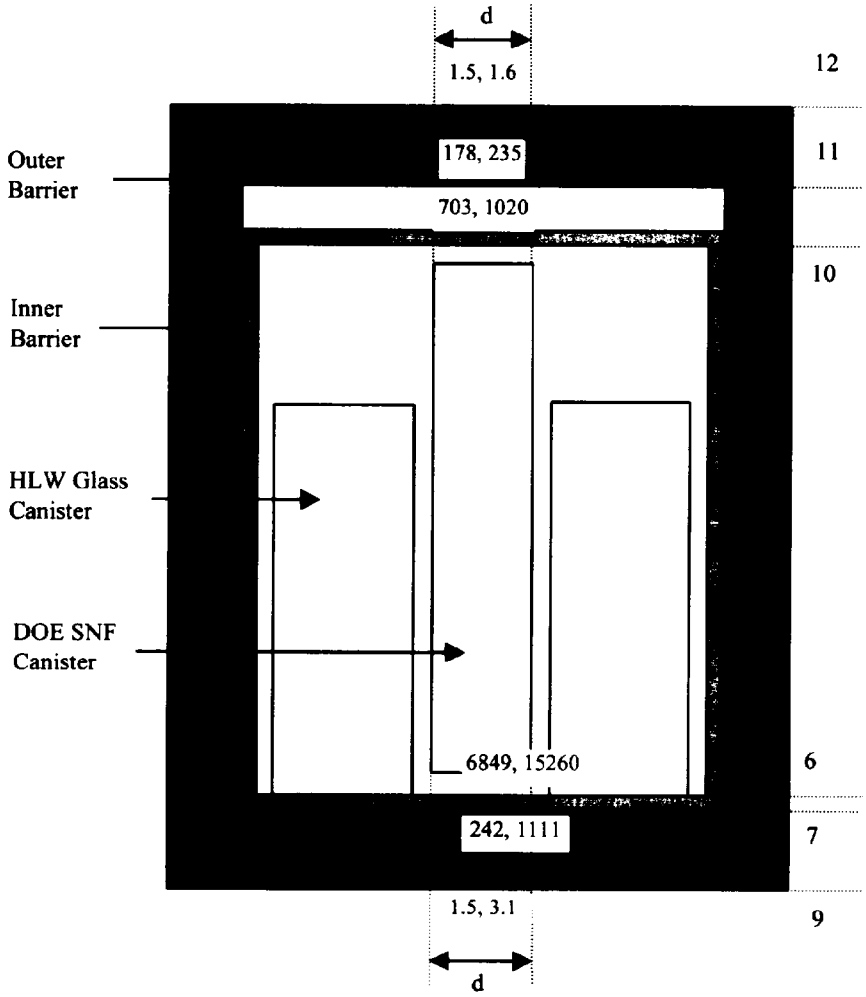

Figure 5-3. MCNP Estimates for Dose Rates in rem/h over Axial Surfaces and Segments

6. DEGRADATION AND GEOCHEMISTRY ANALYSIS

6.1 USE OF COMPUTER SOFTWARE

The EQ3/6 software package originated in the mid-1970s at Northwestern University (Wolery 1992). Since 1978, Lawrence Livermore National Laboratory (LLNL) has been responsible for maintaining of EQ3/6. The software most recently has been maintained under the sponsorship of the Civilian Radioactive Waste Management Program of the DOE. This code identified as CSCI UCRL-MA-110662 V 7.2b, SCR: LSCR198 was obtained from the SCM in accordance with appropriate procedures. The major components of the EQ3/6 package include the following: EQ3NR, a speciation-solubility code; EQ6, a reaction path code that calculates water/rock interaction or fluid mixing in either a pure reaction progress mode or a time mode; EQPT, a data-file preprocessor; EQLIB, a supporting software library; and several supporting thermodynamic data files. The software implements algorithms describing thermodynamic equilibrium, thermodynamic disequilibrium and reaction kinetics. The supporting data files contain both standard-state and activity-coefficient-related data.

EQ6 calculates the irreversible reactions that occur between an aqueous solution and a set of solid, liquid, or gaseous reactants. The code can calculate fluid mixing and the consequences of changes in temperature. This code operates both in a pure reaction progress frame as well as in a time frame.

In this study, EQ3/6 is used to provide:

- A general overview of the nature of chemical reactions to be expected
- The degradation products likely to result from corrosion of the waste forms and canisters
- An indication of the minerals, and their amounts, likely to precipitate within the waste package.

The EQ3/6 calculations reported in this document used the qualified version 7.2b of the code as documented in *EQ3/6 Software Installation and Testing Report for Pentium Based Personal Computers (PCs)* (CRWMS M&O 1998k), and is executed on personal computers (PCs) running Windows 95.

6.2 DESIGN ANALYSIS

6.2.1 Systematic Investigation of Degradation Scenarios and Configurations

Degradation scenarios comprise a combination of features, events, and processes that result in degraded configurations to be evaluated for criticality. A configuration is defined by a set of parameters characterizing the amount, and physical arrangement, at a specific location, of the materials that can significantly affect criticality (e.g., fissile materials, neutron-absorbing materials, reflecting materials, and moderators). The variety of possible configurations is best understood by grouping them into classes. A configuration class is a set of similar configurations whose composition and geometry is defined by specific parameters that

distinguish one class from another. Within a configuration class the values of configuration parameters may vary over a given range.

A master scenario list and set of configuration classes relating to internal criticality is given in the *Disposal Criticality Analysis Methodology Topical Report* (CRWMS M&O 1998a, pp. 3-2 through 3-12) and also shown in Figures 6-1 and 6-2. This list was developed by a process that involved workshops and peer review. The comprehensive evaluation of disposal criticality for any waste form must include variations of the standard scenarios and configurations to ensure that no credible degradation scenario is neglected. All of the scenarios that can lead to criticality begin with the breaching of the waste package, followed by entry of the water, which eventually leads to degradation of the SNF and/or other internal components of the waste package. This degradation may permit neutron absorber material to be mobilized (made soluble) and either be flushed from the waste package or displaced from the fissile material, thereby increasing the probability of criticality.

The standard scenarios for internal criticality divide into two groups:

1. When the waste package is breached only on the top, water flowing into the waste package builds up a pond. This pond provides water for moderation to support a criticality. Further, after a few hundred years of steady dripping, the water can overflow through the hole in the top of the waste package, and flush out any dissolved degradation products.

2. When the waste package breach occurs on the bottom as well as the top, the water flows through the waste package. This group of scenarios allows the soluble degradation products to be removed more quickly, but does not directly provide water for moderation. Criticality is possible, however, if the waste package fills with corrosion products that can add water of hydration and/or plug any holes in the bottom of the waste package. The waste package supports this latter behavior because the silica released by the degrading HLW glass may form clay with enough water of hydration to support criticality.

The standard scenarios for the first group are designated IP-1, -2, -3 (IP stands for internal to the package) according to whether the waste form degrades before the other waste package internal components, at approximately the same time (but not necessarily at the same rate), or later than the waste package internal components. The standard scenarios for the second group are designated IP-4, -5, or -6 based on the same criteria. The internal criticality configurations resulting from these scenarios fall into six configuration classes described below (CRWMS M&O 1998a, pp. 3-10 through 3-12):

1. Basket is degraded but waste form relatively intact and sitting on the bottom of the waste package (or the DOE canister), surrounded by, and/or beneath, the basket corrosion products (see Figure 6-3). This configuration class is reached from scenario IP-3.

2. Both basket and waste form are degraded (see Figure 6-4). The composition of the corrosion product is a mixture of fissile material and iron oxides, and may contain clay. It is more complex than for configuration class 1, and is determined by geochemical calculations as described in Section 6.3.2. This configuration class is most directly reached from standard

scenario IP-2, in which all the waste package components degrade at the same time. However, after many tens of thousands of years the scenarios IP-1 and IP-3, in which the waste form degrades before or after the other components, also lead to this configuration.

3. Fissile material is moved some distance from the neutron absorber, but both remain in the waste package (see Figure 6-5). This configuration class can be reached from IP-1.

4. Fissile material accumulates at the bottom of the waste package, together with moderator provided by water trapped in clay (see Figure 6-6). The clay composition is determined by geochemical calculation, as described in Section 6.3.2. This configuration class can be reached by any of the scenarios, although IP-2 and IP-5 lead by the most direct path; the only requirement is that there be a large amount of glass in the waste package (as in the codisposal waste package) to form the clay.

5. Fissile material is incorporated into the clay, similar to configuration class 4, but with the fissile material not at the bottom of the waste package (see Figure 6-7). Generally the mixture is spread throughout most of the waste package volume, but could vary in composition so that the fissile material is confined to one or more layers within the clay. Generally, the variations of this configuration are less reactive than for configuration class 4, therefore, they are grouped together, rather than separated according to where the fissile layer occurs or whether the mixture is entirely homogeneous. This configuration class can be reached by either standard scenario IP-1 or -4.

6. Fissile material is degraded and spread into a more reactive configuration but not necessarily moved away from the neutron absorber, as in configuration class 3 (see Figure 6-8). This configuration class can be reached by scenario IP-1.

It should be noted that the configuration classes 1, 2, 4, and 5 require that most of the neutron absorber be removed from the waste package; however in configuration classes 3 and 6, the fissile material is simply moved away from the absorber or into a more reactive geometry.

In Sections 6.2.1.1 through 6.2.1.5 the scenarios and the resulting configuration classes that are applicable to the FFTF DOE SNF codisposal waste package are discussed.

Note that most of these configuration pairs (Figures 6-3 through 6-8) look quite different even though both pair members belong to the same configuration class. This apparent dissimilarity arises from the configuration class definition strategy, which classifies critical configurations according to the geometry and composition of the materials, irrespective of the container (either the DOE SNF canister, or the entire waste package).

Note: W.P. = waste package
W.F. = waste form
F.M. = fissile material

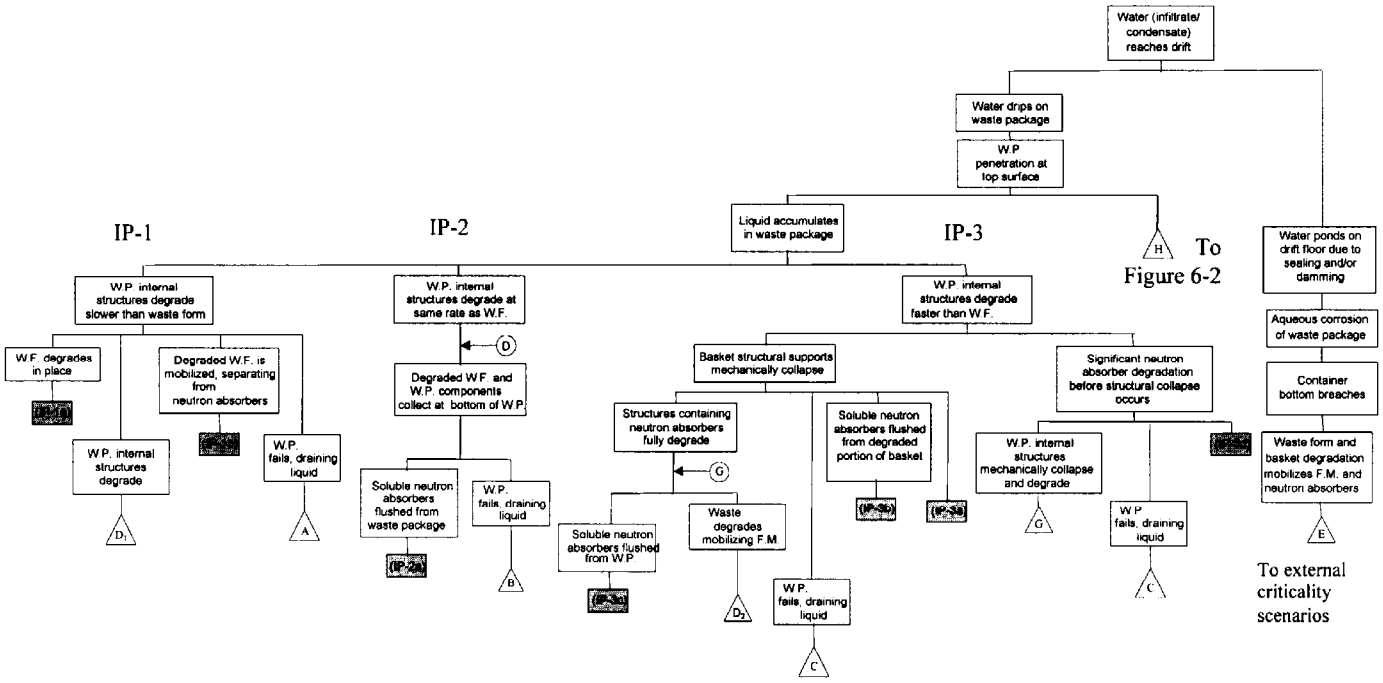

Figure 6-1. Internal Criticality Master Scenarios, Part 1

From Figure 6-1

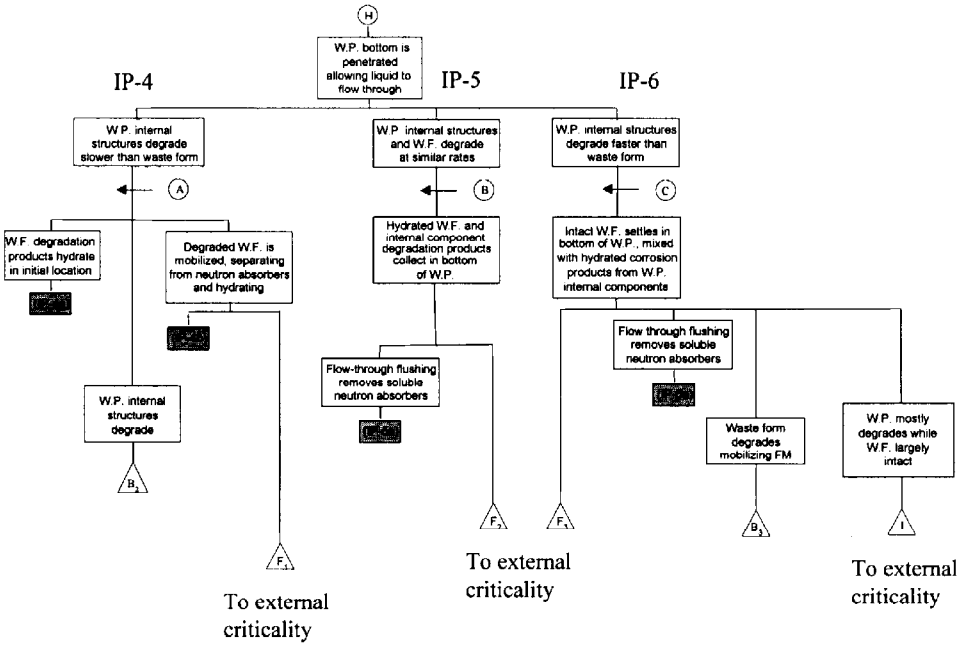

Note: hydrated degradation products may include hydrated metal oxides, metal hydroxides, and clayey materials

Figure 6-2. Internal Criticality Master Scenarios, Part 2

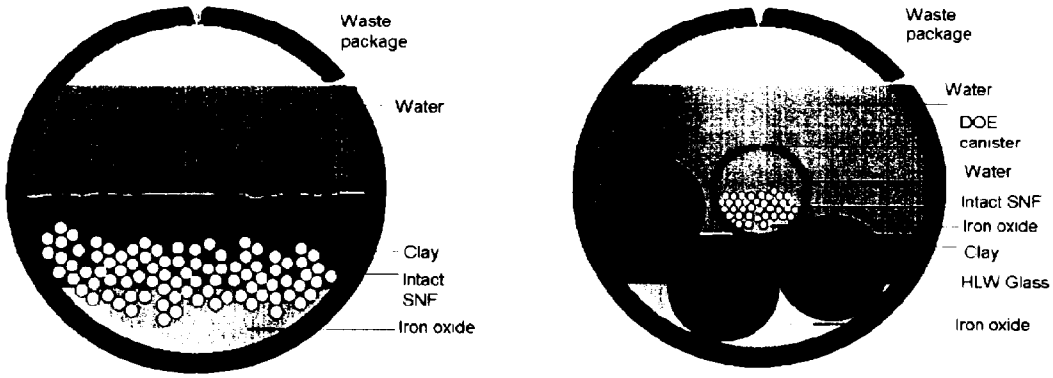

Figure 6-3. Examples of Degraded Configurations from Class 1

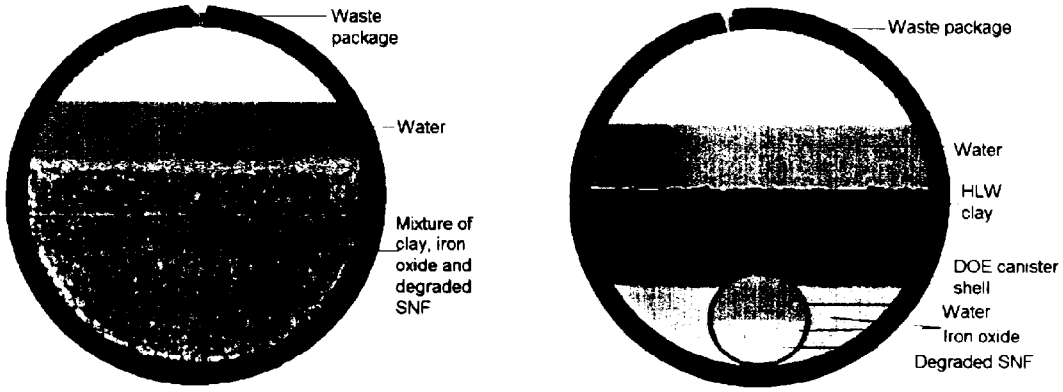

Figure 6-4. Examples of Degraded Configurations from Class 2

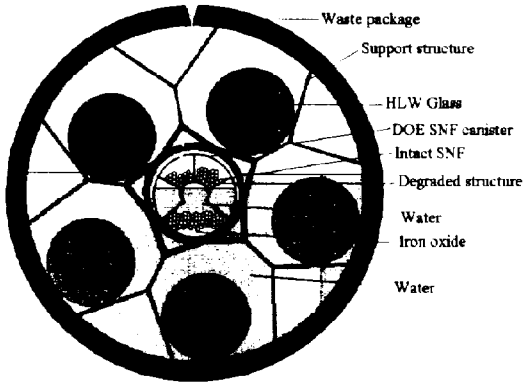

Figure 6-5. Example of Degraded Configurations from Class 3

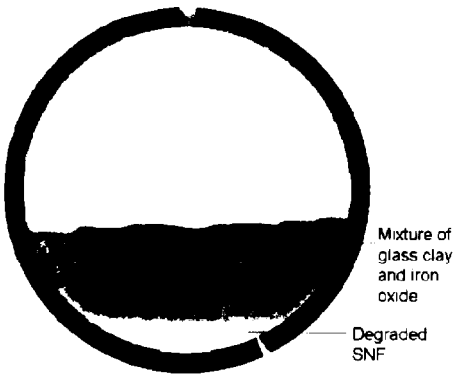

Figure 6-6. Example of Degraded Configurations from Class 4

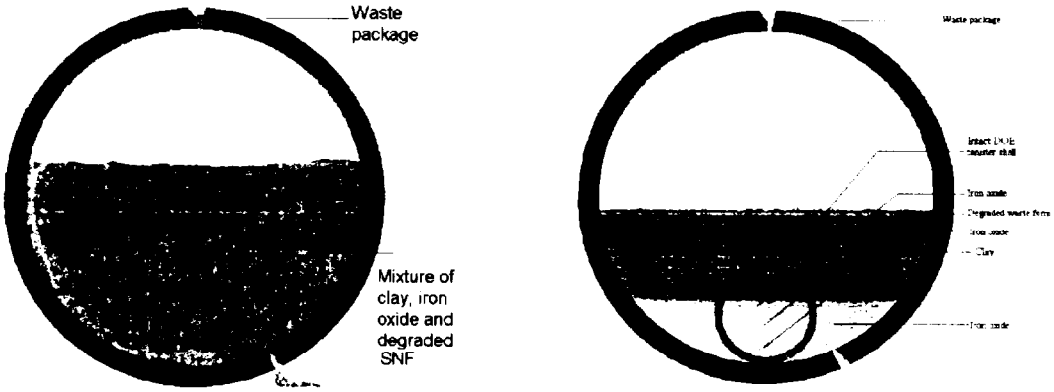

Figure 6-7. Examples of Degraded Configurations from Class 5

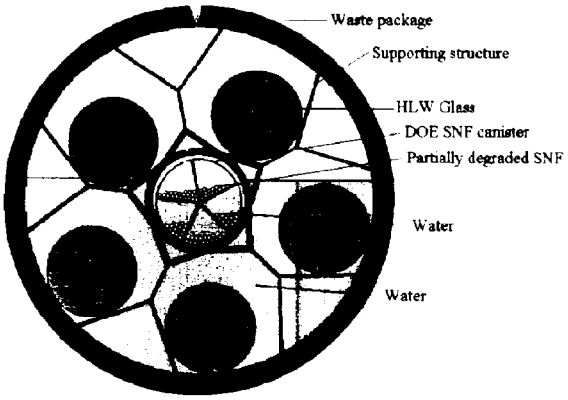

Figure 6-8. Example of Degraded Configurations from Class 6

6.2.1.1 Degraded Assembly (Intact Basket)

For these cases of degraded fuel assemblies within intact basket, the scenarios and configuration classes are applied to the DOE SNF canister and its contents. Since the SNF degrades before the basket in these configurations, this is an example of standard scenario 1. The resultant configurations correspond to refinements of configuration class 3. The varying levels of degradation of DFAs are given by the following sequence, with the section of this report containing the results of the criticality calculations for that configuration shown in parentheses:

1. Degradation of fuel pin clips and spacers (Section 7.4.1)

2. Partial and complete degradation of fuel cladding (Section 7.4.1)

3. Degradation of assembly duct along with fuel pin clips and spacers (Section 7.4.2)

4. Complete degradation of the assembly resulting in pellets stacked randomly in each basket location (Section 7.4.2).

6.2.1.2 Degraded Basket and Intact SNF

Since the basket is more than three times as thick as the FFTF assembly duct, it is virtually impossible for it to completely degrade before the FFTF assembly duct. This configuration is a variation of configuration class 1 and can be reached from standard scenario IP-3 in Figure 6-2. The refinements of this configuration are characterized by the varying levels of degradation of the DFAs and are given in the following sequence, together with the section of this report containing the results of the criticality calculations for that configuration.

1. All DFAs and Ident-69 pin container (if present) are intact (Section 7.4.3).

2. All DFAs are degraded resulting in intact fuel pins stacked inside the DOE SNF canister around an intact Ident-69 pin container (Section 7.4.4).

3. Intact Ident-69 surrounded by a homogeneous mixture resulting from complete degradation of all DFAs and the basket (Section 7.4.5).

4. Degraded Ident-69 mixed with homogeneous mixture resulting from complete degradation of all DFAs and the basket (Section 7.4.6).

5. A homogeneous mixture resulting from complete degradation of six DFAs (the nominal five, plus one replacing the Ident-69 (Section 7.4.6).

Although these configurations are all very unlikely, they are considered for reasons of completeness and conservatism. A more likely set of configurations with some basket degradation would contain some partly degraded basket plates between the remaining assemblies or rods that fall to the bottom of the DOE SNF canister. Such a configuration could arise because of the collapse of the basket structure.

6.2.1.3 Degraded DOE SNF canister Contents and Degraded HLW and other Waste Package Components

In this case, the concepts of scenario and configuration are applied to the entire waste package. These configurations have an intact DOE SNF canister shell surrounded by clay formed by degraded HLW and waste package basket. All DOE SNF canister internals, such as the basket, DFAs, and the Ident-69, if present, are degraded to form a homogeneous mixture. These configurations are from configuration class 5 discussed in Section 6.2.1 and can be reached from any of the standard scenarios shown in Figure 6-2. The calculation of the clay composition is described in Section 6.3.2, and the criticality calculations are described in Section 7.4.8.

6.2.1.4 Completely Degraded DOE SNF canister above Clay from HLW and Waste Package Internals

In this case, the concepts of scenario and configuration are also applied to the entire waste package. These configurations represent the DOE SNF canister as completely degraded and forming a layer above the clay that results from complete degradation of waste package basket and HLW glass canisters. Various combinations of the fuel and clay layers are also investigated. This configuration is a variation of configuration class 5 discussed in Section 6.2.1 and can be reached from standard scenarios IP-4 and -5 shown in Figure 6-2. The calculation of the clay composition is described in Section 6.3.2 and the criticality calculations are described in Section 7.5.1.

6.2.1.5 Clay from HLW and Waste Package Internals above Completely Degraded DOE SNF canister

This case also applies the concepts of scenario and configuration to the entire waste package. These configurations have the clay from the degradation of the waste package basket and HLW glass canisters above the completely degraded DOE SNF canister. This configuration is configuration class 4 discussed in Section 6.2.1 and can be reached from scenarios IP-1 and -4 shown in Figure 6-2. The calculation of the clay composition is described in Section 6.3.2 and the criticality calculations are described in Section 7.5.2.

6.2.2 Basic Design Approach for Geochemical Analysis

The method used for this analysis involves the steps described below.

1. Use the basic EQ3/6 capability to trace the progress of reactions as the chemistry evolves, including estimating the concentrations of material remaining in solution as well as the composition of precipitated solids. (EQ3 is used to determine a starting fluid composition for a series of EQ6 calculations; it does not simulate reaction progress.)

2. Evaluate available data on the range of dissolution rates for the materials involved, to be used as material/species input for each time step.

3. Use the "solid-centered flow-through" mode (SCFT) in EQ6. In this mode, an increment of aqueous "feed" solution is added continuously to the waste package system, and a like volume of the existing solution is removed. This mode simulates a continuously stirred tank reactor.

4. Determine the concentrations of fissile materials in solution as a function of time (from the output of EQ6-simulated reaction times up to $6 \cdot 10^5$ years).

5. Calculate the amount of fissile material released from the waste package as a function of time (which thereby reduces the chance of criticality within the waste package).

6. Determine the concentrations of neutron absorbers, such as Gd, in solution as a function of time (from the output of EQ6 over times up to $6 \cdot 10^5$ years).

7. Calculate the amount of neutron absorbers retained within the waste package as a function of time.

8. Calculate the composition and amounts of solids (precipitated minerals or corrosion products and unreacted package materials).

6.3 CALCULATIONS AND RESULTS

The calculations begin by selecting representative values from known ranges for composition, amounts, and reaction rates of the various components of the FFTF waste package. Surface areas are calculated based on the known package geometry. The input to EQ6 consists of the composition of J-13 well water, together with a rate of influx to the waste package (Section 2.1.8.3). Sometimes the degradation of the waste package is divided into stages (e.g., degradation of HLW glass before breach and exposure of the fuel assemblies and basket materials to the water). The EQ6 outputs include the compositions and amounts of solid products and the solution composition. Details of the results are presented below. The calculation process is described in more detail in CRWMS M&O (1998e).

6.3.1 Gadolinium Solubility Scoping Calculations

If the fissile material were to remain behind in the waste package while the Gd and other neutron absorbers are flushed from the system, an internal criticality could be possible. Uranium and plutonium are quite soluble in alkaline, carbonate-rich solutions produced when the HLW glass degrades (solubility up to ~10^{-1} molal [CRWMS M&O 1998e, p. 38]). The proposed criticality control material, $GdPO_4$, will likely hydrate slightly when exposed to water to form $GdPO_4 \cdot H_2O$. The latter is very slightly soluble in neutral solutions (Firsching, F.H. and Brune, S.N. 1991), though its solubility increases at low and high pHs; complexation at high pH is particularly enhanced by dissolved carbonate (Lee, J.H. and Byrne, R.H. 1992, Figure 8). Conditions of a low pH might be produced as stainless steel degrades separately from the HLW glass. One general scenario that maximizes the potential for internal criticality involves the early breach of the stainless steel Type 304L HLW canisters, followed by the rapid degradation of the HLW glass followed by removal of the alkaline components during a period of relatively high drip rate.

Then the stainless steel Type 316L DOE SNF canister breaches, exposing some of the MOX fuel. In this second stage, the pH of the ambient solutions remains low (~5 to ~6), due in part to the degradation of the stainless steel.

The scenarios chosen for this study build on three previous analyses of the loss of U, Pu, and Gd from waste packages containing fissile waste forms codisposed with HLW glass (CRWMS M&O 1998f; CRWMS M&O 1996b, Table C-1; and CRWMS M&O 1997f, p. 5-17). These prior studies suggested that the greatest removal of Gd would occur at slow drip rates in the second stage described in the previous paragraph. However, the previous work assumed that $GdOHCO_3$ would be the solubility-limiting phase. When $GdPO_4 \cdot H_2O$ is allowed to form, the overall solubility and loss of Gd will be lower. However, as the solubility product of $GdOHCO_3$ includes both hydroxyl and carbonate ions, the solubility of $GdPO_4 \cdot H_2O$ will increase with increasing pH and CO_2 pressure (CRWMS M&O 1998e, p. 26).

Two simplified systems can be used to bound the maximum Gd solubility. For the first system, (called system A) the only source of aqueous Gd and phosphorous (P) would be the dissolution of solid $GdPO_4 \cdot H_2O$, that is, no P is supplied by steel or glass. Such assumptions would be reasonable if the system had been flushed for some time, thus removing the dissolved phosphate contributions from faster-reacting components. Since it could be speculated that such a system would underestimate Gd solubility via aqueous Gd-phosphate complexes, a second system is considered in which aqueous Gd concentration is still controlled by $GdPO_4 \cdot H_2O$, but aqueous phosphate concentration is varied independently. The second system (called system B) is used to estimate the maximum contribution of aqueous phosphate complexes, when other phosphate sources (such as glass and steel) exist. Figure 6-9 shows the Gd species concentrations as a function of pH.

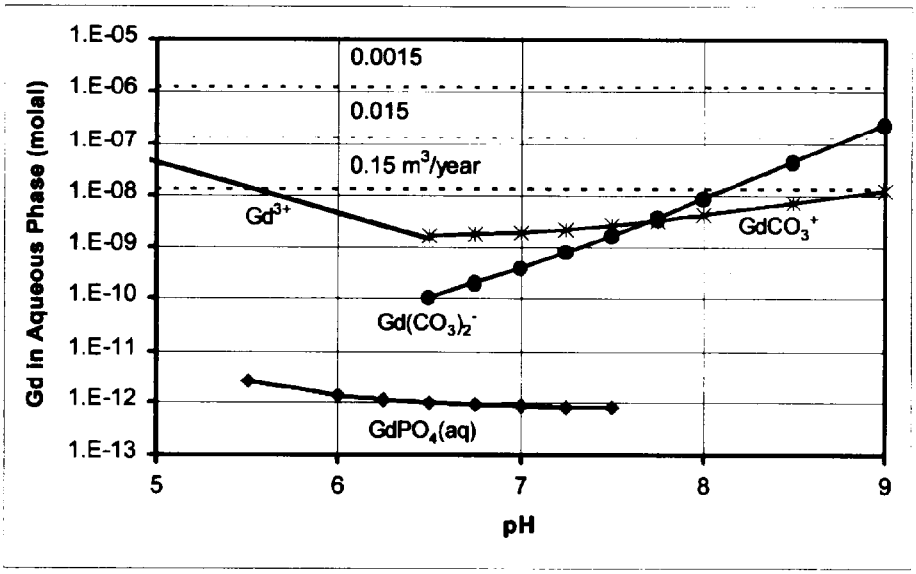

Figure 6-9. Gd Species Concentration as a Function of pH

For system A, at a drip rate of 0.0015 m^3/year (Figure 6-9, top dashed line), the concentrations of all the plotted Gd species are too low to allow significant loss. A "significant" loss is defined as: loss of 10% or more of the total Gd in the waste package over a period of one million years (the National Academy of Sciences recommended evaluation period for the repository). At 0.015 m^3/year (middle dashed line), only $Gd(CO_3)_2^-$ achieves a concentration high enough to cause significant loss, and only with a pH > 8.7 for one million years. However, with the chosen high CO_2 fugacity, the long-term pH will be approximately 7.6 (CRWMS M&O 1998f, Figures 5.3.4-4 through 5.3.4-6). Therefore, it is extremely unlikely that significant loss will occur. (At lower CO_2 fugacities, a higher pH is possible, but the stability of $Gd(CO_3)_2^-$ decreases at lower CO_2 fugacities). At the drip rate of 0.15 m^3/year, Gd^{3+} reaches sufficient concentrations at a pH < 5.5, and $Gd(CO_3)_2^-$ achieves adequate concentrations for loss at a pH > 8. As noted before, the long-term pH is likely to be approximately 7.6, so the latter species is probably not that significant. Previous studies (CRWMS M&O 1998f; and CRWMS M&O 1998e, Figures 5-11 and 5-27) suggest high pH can be achieved when glass degrades rapidly, but at such high drip rates, the period of high pH is limited to thousands, not millions, of years. Similarly, previous studies (CRWMS M&O 1998f, Figure 5.3.2-2; CRWMS M&O 1998e, Figure 5-4) showed that acid conditions (pH < 6) could be produced in the codisposal packages, but generally only for "short" periods ranging over hundreds to tens of thousands of years. Thus, unusual conditions will be required to achieve significant loss of Gd, when the element is present in the package as solid $GdPO_4$.

Figure 6-10 plots the calculated total concentration of dissolved Gd phosphate complexes, as functions of pH and total dissolved phosphate (HPO_4^{2-} and $H_2PO_4^-$), for system B. Even at high total dissolved phosphate (10^{-2} molal), these Gd complexes never exceed concentrations much greater than 10^{-9} molal for 4 ≤ pH ≤ 9, and thus would not result in significant Gd loss from the system.

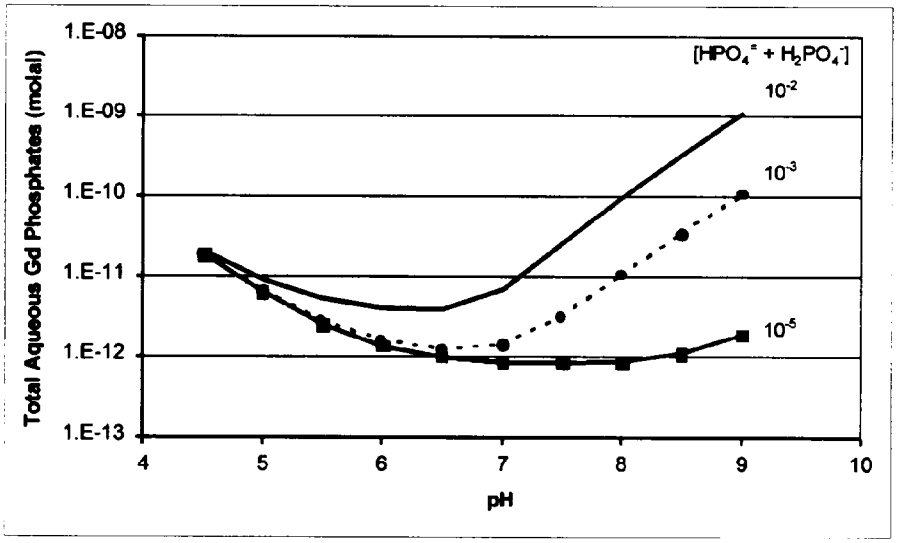

Figure 6-10. Concentrations of Phosphate Species in Equilibrium with $GdPO_4 \cdot 2H_2O$, for Total Phosphate Concentrations of 10^{-5}, 10^{-3}, and 10^{-2} molal

6.3.2 Results of EQ6 Runs

Table 6-1 summarizes the conditions used for the EQ6 runs and the total percentage of Gd, Pu, and U remaining at the end of the runs. Cases 1 through 8 in Table 6-1 all involve simultaneous exposure of the fuel and all package materials to J-13 water; these cases are designed to maximize exposure of the Gd-doped basket to high pH, to stress the enhanced solubility of $GdPO_4$ under alkaline conditions (the right side of Table 6-1). In contrast, cases 9 through 12 all involve two fundamentally different stages. In the first stage, J-13 water interacts with the outside surface of the DOE SNF canister and with all package materials outside the canister (including the glass, stainless steel Type 304L HLW glass pour canister, and the A 516 outer basket). The second stage begins after the HLW glass is completely degraded; the DOE SNF canister is "breached" at the beginning of the second stage, allowing the J-13 water to interact with the fuel assemblies, fuel pin cladding, Gd-doped basket materials, the Ident-69, and the fuel components themselves (the $[U, Pu]O_2$ MOX and UO_2 insulator pellets). Cases 9 through 12 are designed to produce the lowest pH at long times, by removing the alkaline glass before the fuel and Gd-doped basket are exposed. Thus, cases 9 through 12 are intended to test the increased Gd solubility on the left side of Figure 6-9.

Table 6-1. Summary of Geochemistry Results

Case	% Left at End of Run			Rates*				Fe Oxide
	Gd	Pu	U	Steel	Glass	Fuel	J-13	
1	99.9	99.6	56.4	1	1	1	1	hematite
2	99.3	99.0	91.1	1	1	1	2	hematite
3	99.3	97.6	99.7	1	1	1	3	hematite
4	99.8	11.7	11.9	1	2	1	1	hematite
5	99.8	41.4	0.00	2	2	1	1	hematite
6	99.8	41.4	0.00	2	2	2	1	hematite
7	99.7	6.20	1.20	2	2	2	2	hematite
8	99.3	74.5	78.0	2	1	2	2	hematite
9	100	99.5	99.9	2 / 2	2 / 0	0 / 2	4 / 2	hematite
9s**	100	99.7	99.9	2 / 2	2 / 0	0 / 2	4 / 2	hematite
10	100	98.3	99.8	2 / 2	2 / 0	0 / 2	4 / 2	goethite
10s**	100	99.3	99.7	2 / 2	2 / 0	0 / 2	4 / 2	goethite
11	100	98.3	99.9	2 / 2	2 / 0	0 / 2	3 / 1	goethite
12	100	97.0	99.9	1 / 1	2 / 0	0 / 2	3 / 1	goethite

* Rates encoding:
Steels: **1**=average rate; **2**=high rate (Table 2-17).
Glass: **0**=no glass present; **1**=low rate; **2**=high rate (Table 2-18).
Fuel: **0**=no fuel present; **1**=average rate; **2**=high rate (Table 2-19).
J-13: **1**=0.0015 m^3/year; **2**=0.015 m^3/year; **3**=0.15 m^3/year; **4**=0.5 m^3/year (Section 2.1.8.3).
Cases 9 through 12 are multi-stage; rates are given in format: first stage / second stage.
** Glass composition is varied

Both hematite and goethite are observed to form in rust, though the EQ6 thermodynamic database indicates hematite is thermodynamically more stable with increasing temperature. In general, the first stage of a multi-stage run is comparatively short (~10^3 to ~10^4 years) and the second stage of the run is carried out to at least 100,000 years. While the first stage is important in setting up the chemical conditions, the second stage is generally of greater interest for

neutronics calculations, since the corrosion-product compositions can vary greatly in the first stage, but achieve a quasi-steady state composition at long times.

The greatest Gd losses occur in the runs that maximize exposure of Gd to the glass. Nonetheless, the maximum Gd loss is never greater than 0.7% over 100,000 years for any of the scenarios. Furthermore, some of the cases that show some Gd loss also show large losses of Pu and U, which would decrease the potential for an internal criticality.

6.4 SUMMARY

Twelve EQ6 reaction-path cases are constructed to span the range of possible Gd and fuel corrosion (Table 6-1). Two additional cases test the effect of varying glass composition. Cases 1 through 8 test the alkaline regime, achieving high a pH by exposing the fuel to degrading glass. While cases 1 through 8 produce the highest Gd loss, the total loss is $\leq 0.7\%$ in $\geq 100{,}000$ years. Furthermore, when the glass degrades rapidly, the alkaline conditions produce high U and Pu loss (up to 100%), reducing the chances of internal criticality. Some of these "alkaline" cases actually produce a short-lived, very low pH (~3) when glass corrosion rates are set to low values, but steel corrosion rates are set to high values (CRWMS M&O 1998f). These low pH values may not be realistic, since the simple, glass corrosion-rate law does not allow a feedback between pH and corrosion rate (which would tend to increase pH). Cases 9 through 12 test the effect of exposing the Gd, Pu, and U to long-lived acidic conditions (pH ~5 to 6). The highest acidity is obtained by breaking the calculations into two stages. In the first stage, the DOE SNF canister is represented as being intact, and only the outside of the DOE SNF canister, the HLW glass pour canisters (and contained glass), and the A 516 outer basket structure are allowed to interact with the water dripping into the waste package. With a sufficiently high drip rate, the alkaline components of the glass are removed during this stage. In the second stage, the Gd-doped basket, fuel, and other components within the DOE SNF canister are exposed to J-13 water at a much lower drip rate, allowing the pH to drop. When the formation of hematite is suppressed (in favor of goethite), a somewhat lower pH is achieved. None of cases 9 through 12 causes a significant loss of Gd, and none produces more than a few percent loss of either Pu or U.

For two-stage cases, small variations in the Mg content of the glass cause shifts in the times of peak pH and aqueous Gd, Pu, and U concentrations. The cause of these shifts is the production of solid, alkaline-earth carbonates, which consume some of the acid produced by steel degradation and delay the onset of the low-pH plateau. Clays that formed with the Mg-rich glass have higher Mg contents; however, the clay (Mg+Ca+(Na+K)/2)/Si varies by only a fraction of a percent among the cases (as would be expected, since the one-clay phase dominates, and this ratio is fixed by structural and charge balance). The fractions of O, Si, Al, Ti, Fe, Mn, Gd, Pu, and U in the corrosion products are nearly constant (except for the early stages of runs with very low glass corrosion rates), and that overall the variation in glass composition has little effect on the amount of Gd, U, and Pu retained in the waste package. While these results are encouraging, it would be useful to perform a more systematic investigation on the effects of varying glass composition.

The predicted major corrosion products are: an iron-rich smectite clay (nontronite); hematite or goethite; pyrolusite (MnO_2); rutile (TiO_2); and Ni_2SiO_4 or $NiFe_2O_4$. The smectite and hematite

typically comprise more than 90% of the corrosion-product volume. If interaction with J-13 water continues for > 10,000 years, corrosion products may fill approximately 50% of the volume within the CRM. Given the poor packing and high porosity of clay aggregates, the volume fraction occupied by corrosion products plus occluded water may be much greater than 50%. The Gd enters into rhabdophane (hydrated $GdPO_4$) as the basket corrodes, the Pu enters PuO_2, and the dominant U solid is soddyite ($(UO_2)_2(SiO_4)\cdot 2H_2O$).

As the basket corrodes, high aqueous orthophosphate (HPO_4^{2-}) concentrations may be achieved. A somewhat surprising result of this study is the prediction that HPO_4^{2-} complexes may dominate Pu solubility during periods of low pH. However, high levels of dissolved phosphate are not entirely due to the basket; the HLW glass contains about three times the phosphate of the Gd-doped basket, and the abundant carbon steel also contains trace phosphate. Thermodynamic data for Pu orthophosphate are estimated and added to the calculations, but the hypothetical solid does not precipitate, and therefore does not affect solubility. Nonetheless, it would be useful to investigate the sensitivity of the calculations to the quality of the thermodynamic data for the Pu phosphate complexes.

For purposes of the calculations, it is assumed that the most insoluble oxide of Pu could form. This assumption is conservative for internal criticality, but may underestimate the release of Pu from the waste package. As summarized in Stockman 1998, page 625, experiments suggest that the solubility of Pu may be controlled by an amorphous $PuO_2\cdot H_2O$, which is substantially more soluble than PuO_2. Such higher solubility conditions will need to be included in additional EQ6 calculations to develop the source term for external criticality.

The assumption of complete Cr oxidation also bears investigation. The EQ3/6 databases contain very few solids that could precipitate under oxidizing conditions. If such solids exist (e.g., Cr-goethites, Cr-clays, and $CaCrO_4$), the amount of acid production and amount of Cr release from the package may be overestimated. For internal criticality, the assumption of high Cr loss is generally conservative, but these assumptions may be inappropriate when carried through as a source term for external criticality.